

Prediction of directional solidification in freeze casting of biomaterial scaffolds using physics-informed neural networks

Rouhollahi, Amir; Rismanian, Milad; Ebrahimi, Amin; Ilegbusi, Olusegun J; Nezami, Farhad R

DOI

[10.1088/2057-1976/ad7960](https://doi.org/10.1088/2057-1976/ad7960)

Publication date

2024

Document Version

Final published version

Published in

Biomedical Physics & Engineering Express

Citation (APA)

Rouhollahi, A., Rismanian, M., Ebrahimi, A., Ilegbusi, O. J., & Nezami, F. R. (2024). Prediction of directional solidification in freeze casting of biomaterial scaffolds using physics-informed neural networks. *Biomedical Physics & Engineering Express*, 10(6), Article 065023. <https://doi.org/10.1088/2057-1976/ad7960>

Important note

To cite this publication, please use the final published version (if applicable). Please check the document version above.

Copyright

Other than for strictly personal use, it is not permitted to download, forward or distribute the text or part of it, without the consent of the author(s) and/or copyright holder(s), unless the work is under an open content license such as Creative Commons.

Takedown policy

Please contact us and provide details if you believe this document breaches copyrights. We will remove access to the work immediately and investigate your claim.

Green Open Access added to TU Delft Institutional Repository

'You share, we take care!' - Taverne project

<https://www.openaccess.nl/en/you-share-we-take-care>

Otherwise as indicated in the copyright section: the publisher is the copyright holder of this work and the author uses the Dutch legislation to make this work public.

Biomedical Physics & Engineering Express



PAPER

Prediction of directional solidification in freeze casting of biomaterial scaffolds using physics-informed neural networks

RECEIVED
1 May 2024

REVISED
5 September 2024

ACCEPTED FOR PUBLICATION
11 September 2024

PUBLISHED
20 September 2024

Amir Rouhollahi¹ , Milad Rismanian², Amin Ebrahimi³ , Olusegun J Ilegbusi⁴ and Farhad R Nezami¹

¹ Department of Surgery, Brigham and Women's Hospital, Harvard Medical School, Boston, United States of America

² Independent Researcher, Tehran, Iran

³ Department of Materials Science and Engineering, Faculty of Mechanical Engineering, Delft University of Technology, Mekelweg 2, 2628 CD, Delft, The Netherlands

⁴ Department of Mechanical and Aerospace Engineering, University of Central Florida, Orlando, FL, United States of America

E-mail: arouhollahi@bwh.harvard.edu

Keywords: freeze casting, biomaterial scaffold, directional solidification, computational modeling, physics-informed neural networks (PINNs)

Abstract

Freeze casting, a manufacturing technique widely applied in biomedical fields for fabricating biomaterial scaffolds, poses challenges for predicting directional solidification due to its highly nonlinear behavior and complex interplay of process parameters. Conventional numerical methods, such as computational fluid dynamics (CFD), require adequate and accurate boundary condition knowledge, limiting their utility in real-world transient solidification applications due to technical limitations. In this study, we address this challenge by developing a physics-informed neural networks (PINNs) model to predict directional solidification in freeze-casting processes. The PINNs model integrates physical constraints with neural network predictions, requiring significantly fewer predetermined boundary conditions compared to CFD. Through a comparison with CFD simulations, the PINNs model demonstrates comparable accuracy in predicting temperature distribution and solidification patterns. This promising model achieves such a performance with only 5000 data points in space and time, equivalent to 250,000 timesteps, showcasing its ability to predict solidification dynamics with high accuracy. The study's major contributions lie in providing insights into solidification patterns during freeze-casting scaffold fabrication, facilitating the design of biomaterial scaffolds with finely tuned microstructures essential for various tissue engineering applications. Furthermore, the reduced computational demands of the PINNs model offer potential cost and time savings in scaffold fabrication, promising advancements in biomedical engineering research and development.

1. Introduction

The fabrication of porous structures that provide an optimal environment for tissue engineering applications has been a focal point of research in regenerative medicine. Porosity is a vital characteristic of scaffolds, as it not only facilitates cell proliferation but also contributes to mechanical stiffness and controlled drug delivery, making it a key factor in the success of tissue regeneration efforts [1, 2]. The importance of porosity is particularly evident in bone tissue engineering, where studies have shown that the porosity of a scaffold can significantly enhance bone tissue regeneration and promote the differentiation of bone cells

—both of which are crucial for effective tissue integration and healing [3]. Creating scaffolds with the right porous architecture is a complex challenge that requires precise control over the fabrication process. Thus, various advanced techniques have been developed to achieve this, each offering unique advantages in terms of porosity, pore size, and overall scaffold structure. These fabrication methods not only influence the physical characteristics of the scaffolds but also impact their biological performance, making the choice of technique a critical decision in the design of tissue engineering scaffolds. By fine-tuning these methods, researchers aim to develop scaffolds that closely mimic the natural extracellular matrix, thereby

improving the outcomes of tissue engineering applications across various medical fields. Freeze casting, also known as ice-templating, is a manufacturing technique that has emerged to produce three-dimensional porous structures with controlled porosity and interconnected pore structure [4]. The technique has been widely applied to produce biomaterial scaffolds for tissue engineering, regenerative medicine, and drug delivery, among other biomedical fields, as it can support cell adhesion, proliferation, and differentiation, enhancing the overall functionality of the engineered tissues [5]. In addition, providing a suitable porous structure for tissue engineering applications can be achieved through various scaffold fabrication techniques. Among these, the development of porous titanium (Ti) scaffolds has resulted in significant enhancements in both biocompatibility and mechanical properties of the scaffold [6]. Freeze casting, in particular, has proven to be highly effective with bioceramics, making it a key technique in the development of next generation bone graft substitute. This manufacturing technique allows for precise control over the scaffold's microstructure, ensuring that the desired mechanical strength and biocompatibility are maintained, which are crucial for the success of tissue engineering applications [7]. Moreover, the utilization of biocompatible polymers such as chitosan and alginate in scaffold design brings additional advantageous properties. Chitosan, known for its biocompatibility and biodegradability, also offers unique antibacterial properties which prevent infection at the implantation site. Alginate, renowned for its gel-forming abilities, provides a hydrophilic environment that promotes cell proliferation and tissue regeneration. Both materials enhance the immunogenic profile of scaffolds, reducing the body's immune response and increasing the scaffold's functionality in biological environments [8]. It relies on the controlled solidification of a precursor solution or suspension in a mold, followed by controlled sublimation of the solvent under reduced pressure, leading to the formation of a highly ordered porous structure that can mimic the complex architecture of natural tissues [9, 10]. The resultant porous structure can be tailored to specific applications through precise control of parameters, including the size, shape, and orientation of the ice crystals, the concentration and size of the biomaterial particles, and the solidification rate and direction [11–15]. Moreover, this technique preserves the structural integrity of the biomaterials and minimizes the use of potentially harmful chemicals, making it a safer and more sustainable alternative to conventional scaffold manufacturing methods [16, 17].

Producing porous structures with desired microstructural properties through freeze casting requires precise determination of processing parameters and predictive control of the solidification process achieved by adjusting the boundary conditions [18, 19]. However, achieving realizing such control

poses several challenges due to the highly nonlinear behavior of the system, which critically relies on various process parameters and their complex interplay [20]. Optimizing the process parameters for manufacturing biomaterial scaffolds through trial-and-error experiments can be both costly and time-consuming.

The development of analytical and computational models to study complex heat and fluid flow during solidification in freeze casting offers an effective tool for exploring the design space and optimizing the process. While analytical models are generally less time-consuming than computational models, their application is often limited to simple problems such as one-dimensional solidification. High-fidelity numerical simulations can address this limitation by enabling the prediction of the complex solidification process across multiple length and time scales [21–28]. For instance, Muzzio and Dini [29] developed a computational model based on the finite-element (FE) method to determine the thermal profile during freezing for various design parameters (e.g. chamber pressure, initial solution temperature and vial shape), enabling prediction of the average crystal size based on these parameters. Similarly, Husmann *et al* [30] performed FE-based thermal simulations to investigate the impact of mold design on the structure of freeze-casted scaffold materials and showed that the scaffold pore structure can be manipulated by modifying both the geometry and material of the mold. Rouhollahi *et al* [31] developed a computational fluid dynamics (CFD) model that combined heat and fluid flow models. Incorporating a population balance model, they predicted the crystallization pattern and average pore size in freeze-casted chitosan-alginate scaffolds within molds of varying diameters and heights. Additionally, Cyr *et al* [32] employed an FE-based thermal model to predict the evolution of the thermal field in a mold and the topology of the solidification front in freeze casting.

In recent years, high-fidelity physics-based numerical simulations have emerged as a promising tool for predicting thermal field evolution and solidification processes during freeze casting. However, these simulations require special consideration of convergence stability issues and frequently demand substantial computational resources, posing challenges for their practical application in process optimization. Additionally, defining the physical problem often hinges on oversimplified boundary conditions, primarily due to the challenges associated with obtaining precise and non-intrusive measurements of these conditions. Recent advancements in the field of artificial intelligence (AI) present remarkable potential for the development of surrogate models [33–37], which can expedite the prediction of thermal field evolution during freeze casting, even with limited knowledge of the boundary conditions.

To overcome the limitations of high-fidelity physics-based numerical simulations, we have developed a

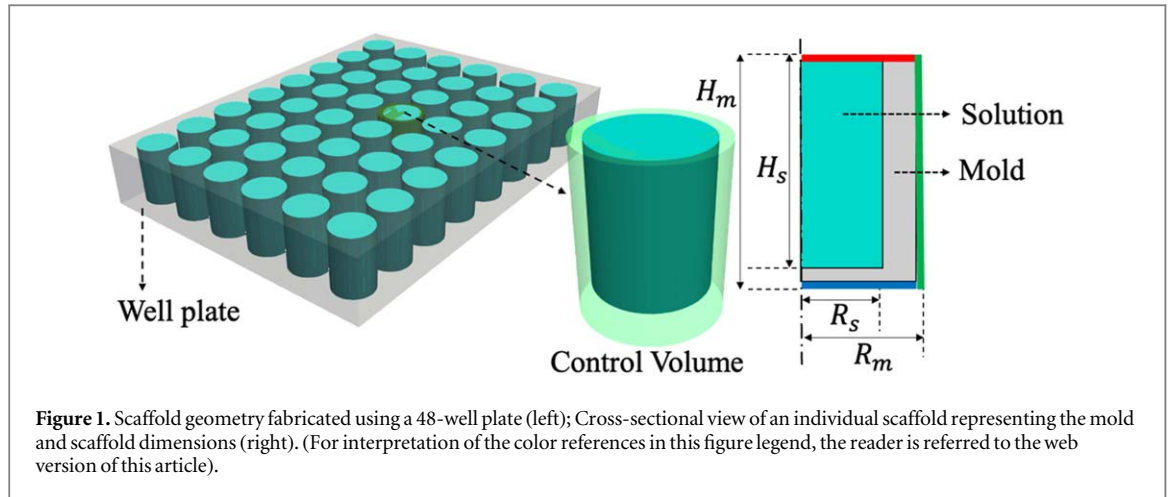


Figure 1. Scaffold geometry fabricated using a 48-well plate (left); Cross-sectional view of an individual scaffold representing the mold and scaffold dimensions (right). (For interpretation of the color references in this figure legend, the reader is referred to the web version of this article).

Table 1. The thermophysical properties of chitosan-alginate solution and polystyrene [31].

Property	Chitosan-alginate solution	Polystyrene
Thermal diffusivity, α ($\text{mm}^2 \text{s}^{-1}$)	0.14	150
Melting temperature, T_m (K)	273.15	—
Latent heat of fusion, L (kJ kg^{-1})	330	—

model based on physics-informed neural networks (PINNs) to predict the unsteady solidification process in the mold using only a few points on the boundary. To generate the data required for training the PINNs model, we developed a physics-based computational model based on CFD to predict the thermal field in the mold. The PINNs model then predicts the entire thermal field and its evolution in the mold for arbitrary experimental conditions, using data obtained from only a few temperature probes. This approach represents a novel solution to the challenges associated with high-fidelity numerical simulations and oversimplified boundary conditions. By employing a PINNs model, the present work significantly mitigates the computational costs associated with the process optimization while providing accurate predictions of the solidification process. The outcomes of the PINNs model were validated against the results of the high-fidelity physics-based thermal model, demonstrating the effectiveness of the proposed approach.

2. Problem description and methodology

The size and morphology of pores in biomaterial scaffolds produced using freeze-casting are significantly influenced by the evolution of the thermal field during production. In this study, a numerical investigation was conducted to analyze the evolution of thermal fields in freeze-casting of a 48-well plate (figure 1). The used solution material was a mixture of chitosan and alginate (CA), which is widely employed for fabricating biocompatible scaffolds [38]. The mold employed in this process was made of polystyrene. Table 1 provides the thermophysical properties of

both the CA solution and polystyrene used in the simulations. To produce the scaffolds, the well plate mold was subjected to a temperature of -20°C for twelve hours. During this period, the solution in the mold undergoes solidification, resulting in the nucleation and growth of ice crystals that expel the particles to the interstitial spaces. Subsequently, the ice crystals were sublimated in a freeze-dryer, resulting in a porous structure that represents the final microstructure of the scaffold.

The effects of mold geometry and thermophysical properties of the mold material and the solution on the thermal field evolution were investigated. To simplify the problem and reduce the calculation time, a single well with axisymmetric well was modeled as a control volume. This modeling approach inherently assumes a symmetry condition between the wells, implying that each well in the system behaves and interacts in a similar manner. This assumption is crucial for simplifying the computational model and is a key consideration in interpreting the results. The control volume has a height (H_m) of 20 mm and a radius (R_m) of 10 mm. The solution container in the control volume has a height of H_s and a radius of R_s . Since the fluid flow within the solution is negligible during the freeze-casting process, heat conduction is assumed to be the dominant mode of heat transfer. Accordingly, the governing equation for the conservation of energy is expressed as follows:

$$\frac{1}{\alpha} \frac{\partial T}{\partial t} = \frac{1}{r} \frac{\partial}{\partial r} \left(r \frac{\partial T}{\partial r} \right) + \frac{\partial^2 T}{\partial z^2}, \quad (1)$$

where, T is the temperature, r the radial coordinate, z the axial coordinate, and α the thermal diffusivity of the material. Thermal diffusivity, which is calculated

Table 2. Grid independent study.

Number of cells	t (s)						RMSE
	0	500	1000	1500	2000	2500	
100	276	272.37	270.83	269.37	267.62	263.16	0.399437
200	276	271.96	270.48	269.08	267.38	262.76	0.105987
400	276	271.95	270.47	269.06	267.3	262.63	0.044159
800	276	271.95	270.45	269.02	267.26	262.54	—

by dividing the thermal conductivity by the product of the density and heat capacity, can be determined as follows:

$$\alpha = \begin{cases} \frac{k_m}{\rho_m \times c_{p,m}} & \text{not } (r \langle \beta_r R \text{ and } z \rangle \beta_z H) \\ \frac{k_l}{\rho_l \times c_{p,l}} & (r \langle \beta_r R \text{ and } z \rangle \beta_z H) \text{ and } (T > T_m) \\ \frac{k_s}{\rho_s \times c_{p,s}} & (r \langle \beta_r R \text{ and } z \rangle \beta_z H) \text{ and } (T < T_m) \end{cases} \quad (2)$$

where, the terms R , H , k , ρ , and c_p , represent radial distant from the axisymmetric axis, vertical distance from the bottom of the mold, thermal conductivity, density, and specific heat capacity, respectively. The subscripts ‘m’, ‘l’, and ‘s’ refer to the properties of the mold, the liquid scaffold, and the solid scaffold, respectively. The size of the scaffold relative to the mold is defined by using the parameters $\beta_r = \frac{R_s}{R_m}$ and $\beta_z = \frac{(H_m - H_s)}{H_m}$. Accordingly, for a fixed mold design, the radius of the scaffold (R_s) increases with increasing β_r , and the height of the scaffold (H_s) decreases with increasing β_z .

The governing equation for heat conduction at the interfaces between the mold-scaffold and the solid-liquid can be expressed as follows:

$$-k_m \frac{\partial T}{\partial n} = -k_{s,l} \frac{\partial T}{\partial n}, \text{ for scaffold - mold interface} \quad (3)$$

$$-k_s \frac{\partial T}{\partial n} - k_l \frac{\partial T}{\partial n} = \rho_{s,l} L \frac{ds(t)}{dt}, \text{ for solidification interface} \quad (4)$$

where, L represents the latent heat of the scaffold material and n signifies the direction normal to the interface. The primary challenge in resolving freezing issues lies in the uncertainty of the freezing front’s position at any given time, which leads to ambiguity regarding which heat conduction equation applies at each moment.

The boundary conditions for the energy conservation equation are as follows: the outer vertical surface of the control volume, shown by the green line in figure 1, was thermally insulated. A constant temperature of -20°C was set at the bottom surface of the control volume, shown by the blue line in figure 1. The top surface of the control volume, shown by the red line in figure 1, experienced convective heat losses with a heat transfer coefficient of $10 \text{ W m}^{-2} \text{ K}^{-1}$ and a free

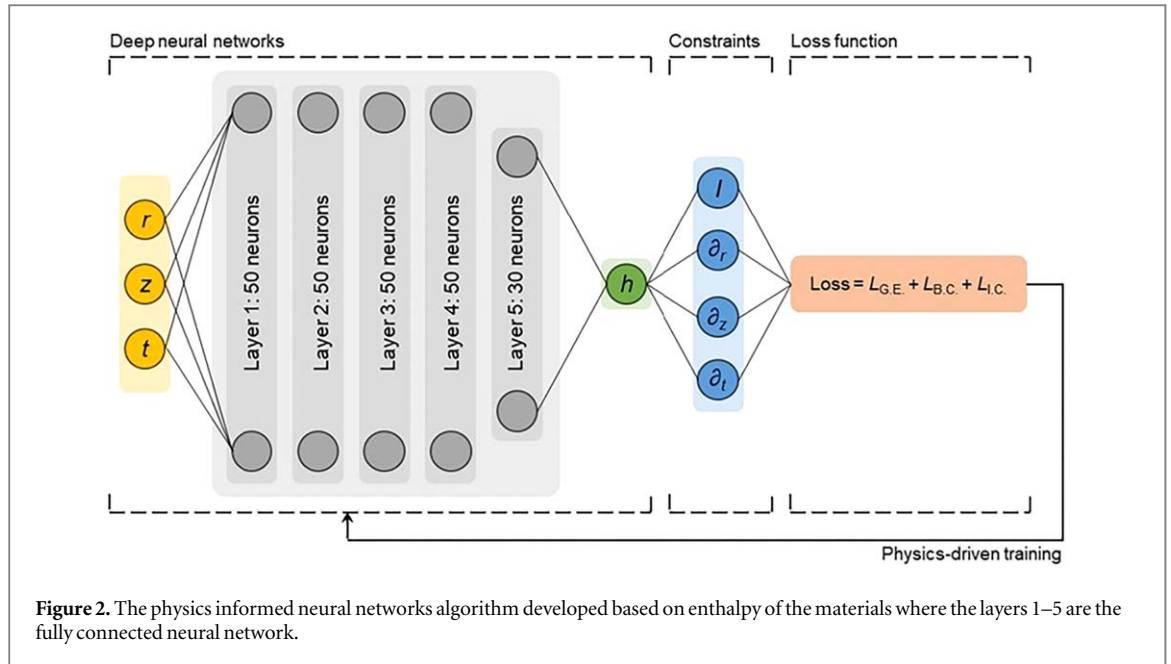
stream temperature of -20°C [31]. The initial temperature of both the mold and the solution was 4°C .

The developed physics-based CFD model was implemented in ANSYS Fluent (ANSYS, Inc., Canonsburg, PA, USA) to predict the solution of the unsteady conjugated heat transfer problem described in this study. The computational domain was discretized using uniform quadrilateral cells with a cell size of 0.5 mm. Spatial discretization of the energy equation was performed using the second-order upwind scheme. A first-order implicit scheme was used for temporal discretization and the time-step size was set to 0.05 s. Average temperature was quantified to confirm grid independency (table 2). The root mean square error (RMSE) of the results is defined as $RMSE_i = \sqrt{\frac{\sum_{time=0}^{time=2500} (T_i - T_{800})^2}{N}}$ where $N = 6$. RMSE values suggested that grid independence is achieved beyond 200 cells, where further increase in number of cells did not significantly enhance accuracy. Therefore, a cell number of 200 was selected for subsequent computations, offering a balance between computational accuracy and efficiency.

2.1. Physics-informed neural networks

Following the description of the model utilizing Physics-Informed Neural Networks (PINNs), figure 2 provides a detailed visual representation of the model’s architecture. It began with an input layer assuming the values of time and space, which then fed into five neural network layers. These layers were intricately connected to physical constraints that embodied the enthalpy of the mold and solution in both liquid and solid states. At the end of this architecture, there is a focus on the physics-informed loss function, which integrates the physical constraints with the neural network’s predictions to ensure that the output adheres closely to the underlying physical laws.

Once trained, PINNs offered a method with significantly reduced computational demands, capable of predicting key physical properties like enthalpy and temperature across the domain. The inputs for this PINNs model included the position vector \mathbf{r} (encompassing r and z) and time t , while its output was the enthalpy corresponding to the given (\mathbf{r}, t) coordinates. The two-dimensional spatial coordinates were considered as $\mathbf{r} = (r, z)$ for the PINNs model and the temperature distribution function was defined as $h = (t, \mathbf{r})$. Temperature was the output variable of the neural networks in common PINNs models for predicting its



temporal map, but the enthalpy was chosen here as the output variable because it enables the governing equation (equation (1)) to be readily transformed to equation (3) with each of equation (2)’s conditions hold according to the input parameters (t, r).

The architecture comprised a fully connected neural network with a 5-layer structure. The network employed a sigmoid activation function and was tailored to predict the enthalpy as the output variable.

indicating the predicted and actual temperature values, respectively.

To calculate the N_p as the prediction governing equation:

$$N_p = \chi - \frac{\partial h}{\partial t}, \tag{5}$$

where,

$$\chi = \begin{cases} \alpha_{mold} \left[\frac{1}{r} \frac{\partial}{\partial r} \left(r \frac{\partial h}{\partial r} \right) + \frac{\partial^2 h}{\partial z^2} \right], & \text{not } (r \langle \beta_r R \text{ and } z \rangle \beta_z H) \\ \alpha_l \left[\frac{1}{r} \frac{\partial}{\partial r} \left(r \frac{\partial h}{\partial r} \right) + \frac{\partial^2 h}{\partial z^2} \right], & (r \langle \beta_r R \text{ and } z \rangle \beta_z H) \text{ and } (h_l < h) \\ \alpha_l \left[\frac{1}{r} \frac{\partial}{\partial r} \left(r \frac{\partial h}{\partial r} \right) + \frac{\partial^2 h}{\partial z^2} \right], & (r \langle \beta_r R \text{ and } z \rangle \beta_z H) \text{ and } (h < h_s) \\ \alpha_1 \frac{1}{r} \frac{\partial}{\partial r} \left(r \frac{\partial h}{\partial r} \right) + \alpha_2 \frac{\partial^2 h}{\partial z^2}, & (r \langle \beta_r R \text{ and } z \rangle \beta_z H) \text{ and } (h_l < h < h_s) \end{cases} \tag{6}$$

The loss function (Loss) was expressed as the sum of and three constituent terms:

1. $L_{G.E.} = \text{MSE}(N_p, 0)$ represents the loss associated with the governing equations, where MSE denotes the mean square error, and N_p corresponds to the predicted value.
2. $L_{B.C.} = \text{MSE}(T_p, T_a)_{B.C.}$ represents the loss related to the boundary conditions, with T_p and T_a indicating the predicted and actual temperature values, respectively.
3. $L_{I.C.} = \text{MSE}(T_p, T_a)_{I.C.}$ represents the loss originating from the initial conditions, with T_p and T_a

$$\alpha_1 = \begin{cases} \alpha_l \frac{\partial h}{\partial r} > 0 \\ \alpha_s \frac{\partial h}{\partial r} < 0 \end{cases} \quad \alpha_2 = \begin{cases} \alpha_l \frac{\partial h}{\partial z} > 0 \\ \alpha_s \frac{\partial h}{\partial z} < 0 \end{cases} \tag{7}$$

The calculation of partial derivatives of enthalpy with respect to space and time can be accomplished through the utilization of auto-differentiation in neural networks. This methodology employs the chain rule to compute

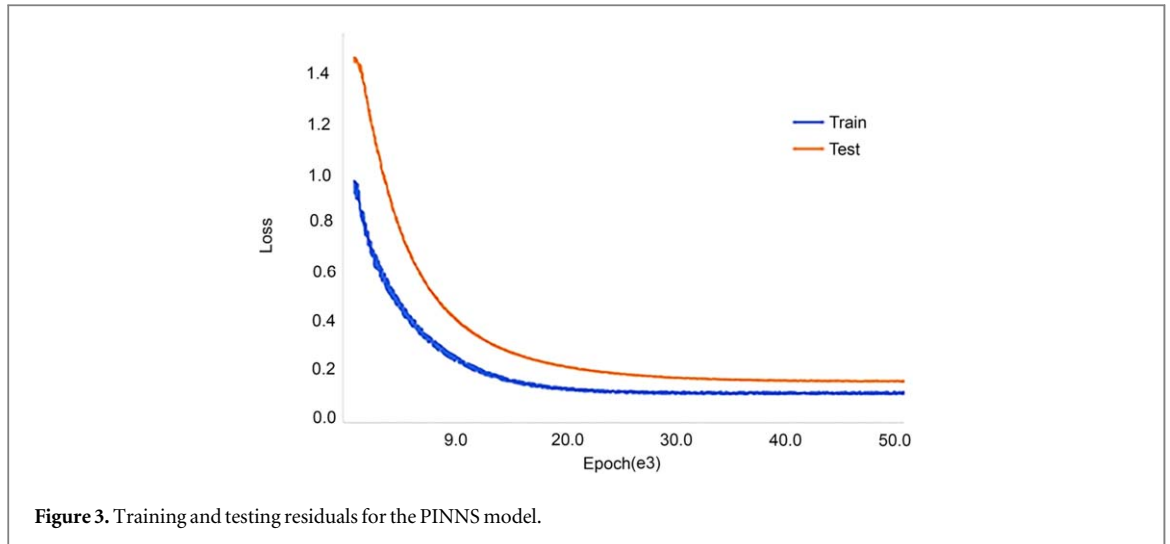


Figure 3. Training and testing residuals for the PINNS model.

derivatives analytically and efficiently during the back-propagation process. Hence, the derivatives can be computed at any point within the domain by PINNs, eliminating the necessity for information from neighboring points, as required by CFD solvers. This characteristic represents a notable advantage of PINNs over conventional numerical methods employed for solving partial differential equations.

A total of 100000, 5000, and 150 points were randomly selected for the computation of $L_{G,E}$, $L_{B,C,s}$, and $L_{I,C}$, respectively. Subsequently, 50000 epochs were executed on a personal computer equipped with an Intel Core i9 CPU and an NVIDIA 4090 GPU. It's important to note that the mentioned 250,000 data points were derived from CFD simulations and not directly used for training the PINNs. We utilized a selected subset of these data points to train the PINNs efficiently. This selection was strategically made to optimize the training of the PINNs model, prioritizing the capture of the system's critical dynamics while avoiding unnecessary complexity that could lead to overfitting. By carefully curating these data points, we aimed to strike a balance between model efficiency and accuracy. Additionally, the chosen data points are representative of the broader dataset, ensuring that the trained model can generalize effectively across the full spectrum of operational conditions. This approach enhances the model's robustness and reliability in predicting system behavior under varied scenarios. The predicted temperature distribution generated by the PINNs model was compared with the temperature distribution obtained from the numerical simulations based on CFD to validate the PINNs model. Figure 3 displays the training and testing residuals, indicating the convergence of the simulation and the satisfactory validation of the PINNs tool.

3. Results and discussion

In the initial phase of validation for the proposed PINNs model, the examination of mold cooling and

subsequent scaffold freezing was conducted through the numerical simulation based on the CFD model, as outlined in section 2. The outcomes of this analysis are detailed in section 3.1. In the subsequent sections 3.2 and 3.3, the effects of thermal conductivity of the mold and dimensions of the scaffold on the temporal and spatial distribution of temperature are presented, respectively. The results to be presented in the subsequent sections were derived using the PINNs model developed in the present study.

3.1. Verification of the developed PINNs model

The problems of heat transfer and freezing of the scaffold and mold were studied using both the PINNs and the CFD models. Figure 4 shows the temperature distribution in the scaffold from left to right at 500 s, 1500 s, and 2500 s after the boundary conditions are applied.

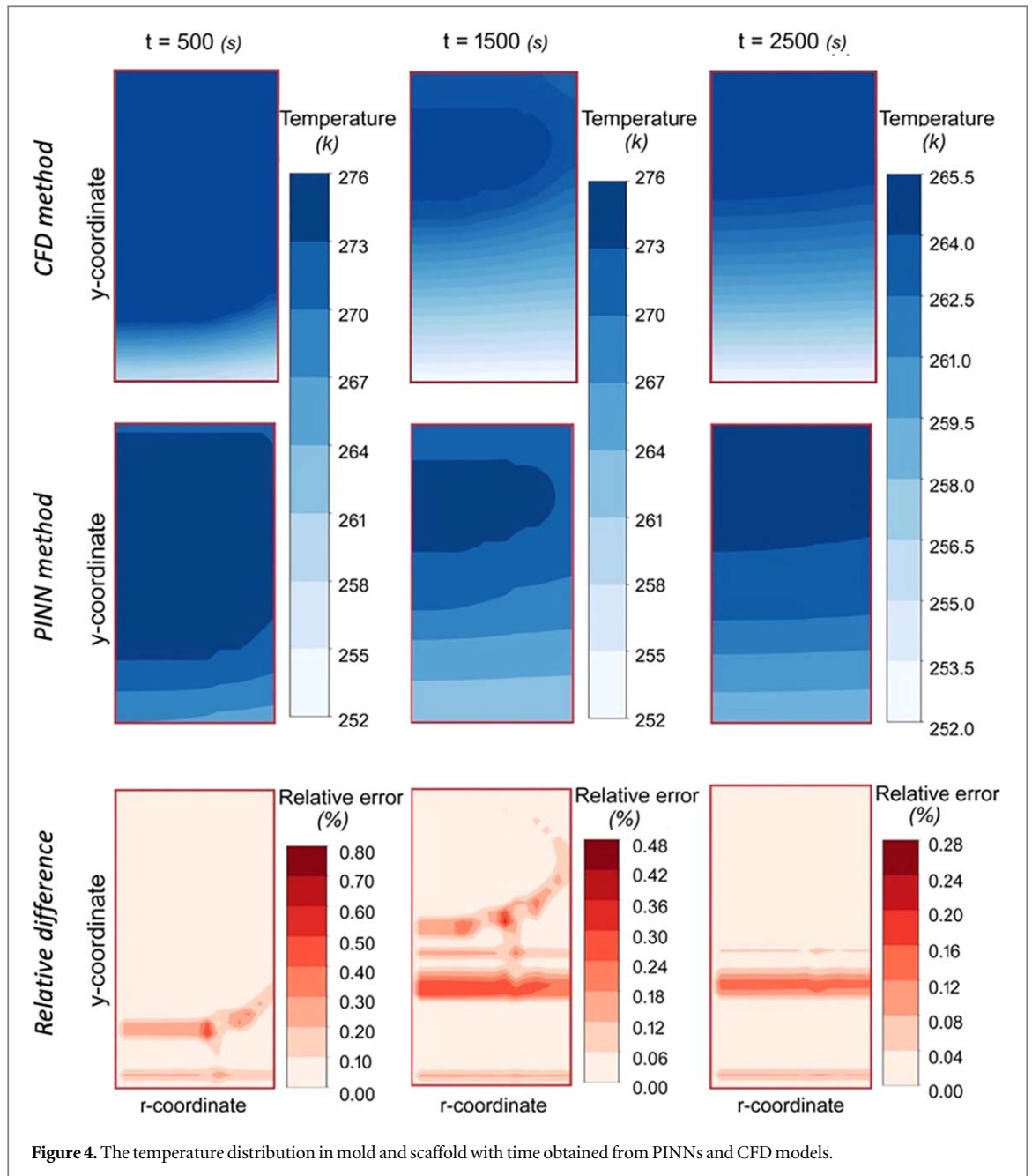
The relative difference, D_{rel} , at each point is defined as follows:

$$D_{rel} = \frac{|T_{PINNs} - T_{CFD}|}{T_{CFD}} \quad (8)$$

where T_{PINNs} and T_{CFD} are temperature measurements from PINNs model and CFD model at that point.

The results of the numerical simulation based on CFD (shown in top row) are compared with the results obtained from the PINNs model (middle row), and the D_{rel} values between the two modeling approaches are shown in the bottom. The relative difference at each point is defined as the percentage difference between the temperature values obtained from the PINNs model and CFD at that point, relative to the latter.

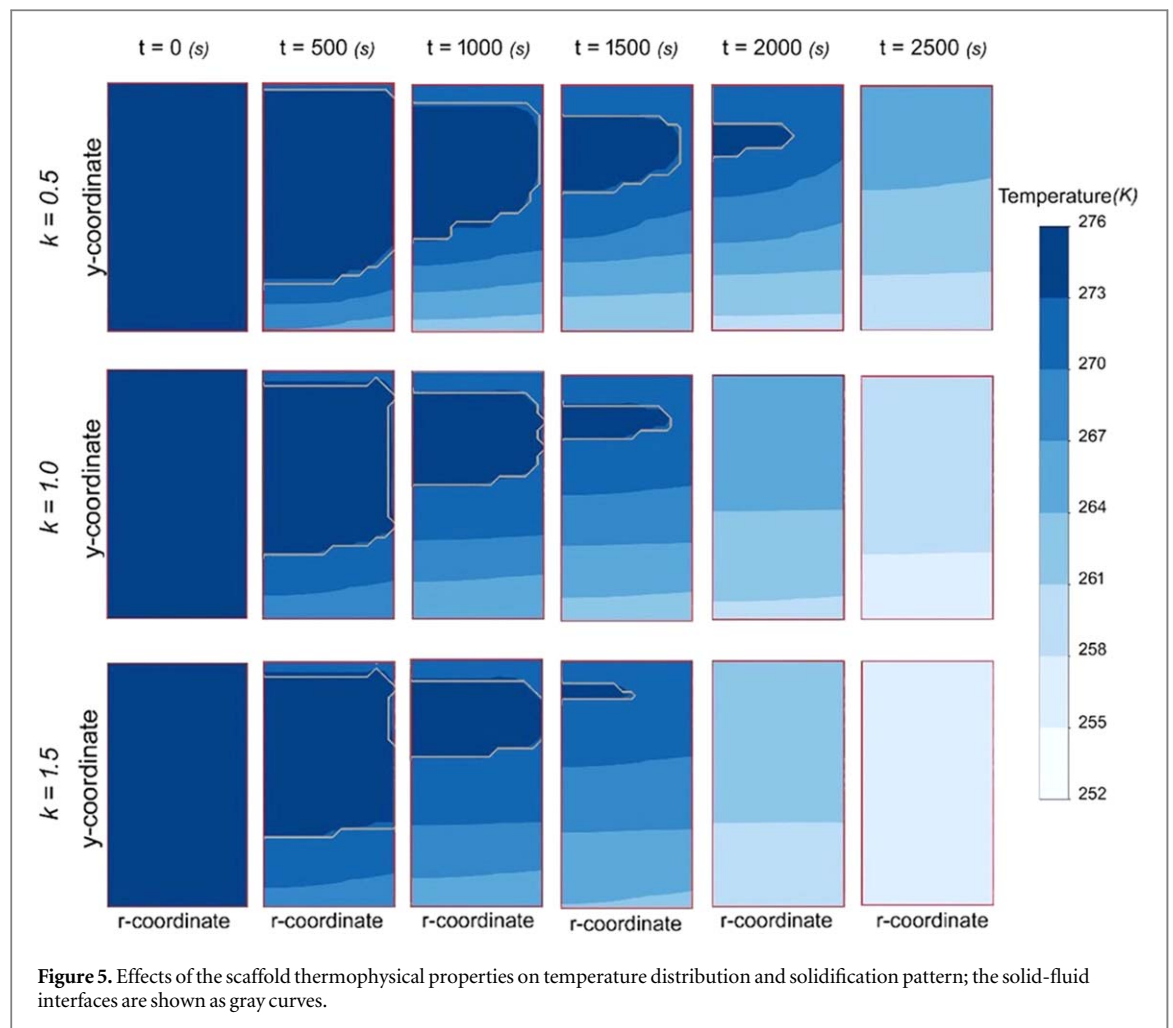
The results obtained from both the PINNs and CFD indicate that the liquid phase of the scaffold has decreased from 73% volume at 500 s to 12% volume at 1500 s. Moreover, the solution is entirely solidified after 2500 s. Heat is transferred primarily from the bottom surface of the scaffold, and the last part of the scaffold to solidify is the layer close to the upper (free)



surface. This trend is attributed to the higher heat conduction through the mold at the bottom than the natural convective heat transfer at the upper surface of the scaffold. Therefore, the initiation of the solid crystal in the final scaffold triggered from the bottom of the scaffold can cause a gradient in crystal size from bottom to top due to the varying cooling rates, with finer crystals forming at the bottom where cooling is more rapid and larger crystals forming near the top. This can affect the mechanical properties of the scaffold, such as its strength and rigidity, which are critical in applications where the scaffold is used for load-bearing purposes. To ensure uniform properties throughout the scaffold, controlling the temperature gradient during the solidification process is crucial.

The results presented in figure 4 also demonstrate a reasonable agreement between the outcomes

obtained from the PINNs and CFD models in predicting the temperature field with the maximum deviation of 0.8%, 0.48%, and 0.28% at 500 s, 1500 s, and 2500 s, respectively. In the PINNs approach, as outlined by equations (5)–(7), the criterion for the diffusion of information in enthalpy computations dictates that the largest D_{rel} within each contour is associated with regions experiencing the steepest gradient in enthalpy. By comparing the D_{rel} percentage and the temperature distribution contours, the relative agreement between the location of the maximum relative difference percentage and the solid–liquid interface can be determined. The high enthalpy gradient in regions where solid–liquid phase transformation takes place has obviously led to computational difference in the PINNs model. Additionally, the maximum percentage



of D_{rel} has decreased from 500 s to 2500 s with the reduction of the magnitude of enthalpy gradient.

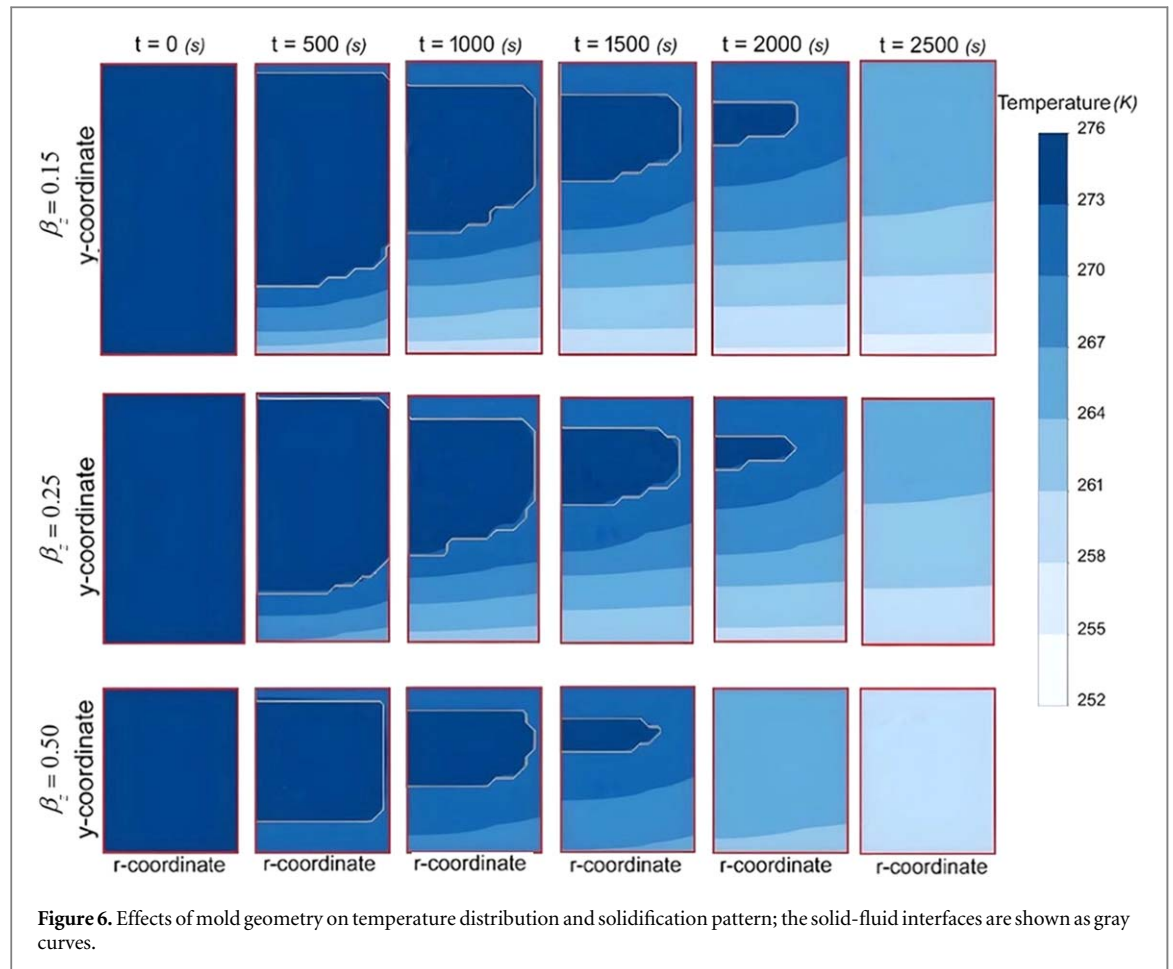
The small values of D_{rel} throughout the domain promise high accuracy of the predictions, which can be beneficial for designing biomaterial scaffolds with precise microstructural characteristics. As a limitation of the developed PINNs model, despite low deviation percentages indicating a generally good match between the CFD and PINNs models, the greatest errors occur at the phase change boundary. This is due to the formation of concentration and enthalpy gradients in that area, leading to inaccuracies. Consequently, using the PINNs method for precise temperature measurements near the phase change boundary may result in significant errors, although predictions elsewhere align well with the CFD model.

The proper matching of the results obtained from the PINNs model and CFD, as well as the low percentage difference between the temperature contours, indicate the validity of the proposed PINNs model. Therefore, in the following sections, the effect of geometric and physical parameters of the scaffold on the freezing process will be investigated using this validated method. Since the formation of scaffold pores is related to the crystal formation during the freezing process, in the sections that follow, we will investigate

the effects of mold thermal distribution and mold geometry on the crystallization process. It should be noted that in the following discussions, the terms crystals and scaffold pores will be used interchangeably [31].

3.2. Effect of the scaffold thermophysical properties on solidification

The effects of the scaffold thermophysical properties on temperature distribution and solidification pattern were studied (figure 5). The results of the PINNs model indicate that the higher conductivity of the solution leads to a more unidirectional solidification. The establishment of unidirectional solidification can be attributed to the enhanced thermal diffusivity of the scaffold material, suggesting an approximately uniform crystal size [39]. The temperature gradient indicates that at any cross section (r varying while y is constant) the crystal size will be smaller closer to the mold wall because of the higher temperature gradient and consequently less time is required for crystal growth. In addition to the smaller crystal size, the rapid cooling at locations closer to the mold centerline results in a more random orientation of the crystals due to the nucleation of multiple grains [40]. In molds with higher thermal diffusivity, the solidification time is reduced because these molds can transfer heat more



efficiently. This rapid heat transfer allows the material inside the mold to cool down and solidify faster. Conversely, in molds with lower thermal diffusivity, heat is transferred more slowly. This slower heat transfer rate affects the temperature distribution during the freezing process, leading to a higher temperature gradient. Such a high gradient, in turn, results in smaller crystal sizes and more random orientations throughout the material, as different regions solidify at different rates [41].

3.3. Effect of mold geometry on the solidification rate

The effects of mold geometry on temperature distribution and solidification patterns, predicted using the PINNs model, were also explored (figure 6). The smaller values of β_z results in a more unidirectional solidification as the temperature gradient at the bottom of the mold is higher for molds with larger β_z values. It is also observed that smaller values of β_z are associated with higher temperature gradients at every time step, indicating a smaller crystal size and a more random orientation of the crystals. However, a larger β_z value results in a quicker solidification, which leads to a larger and more uniform crystal formation. This in turn, leads to a more uniform pore size and higher porosity in the fabricated scaffolds, offering a more

superior performance for the scaffold in cell seeding and drug delivery applications.

Although this research provides novel insights and advancements in the application of physics-informed neural networks (PINNs) to design bioscaffolds, there are certain limitations to be acknowledged. First, scaling the current model to extremely complex systems remains a challenge, potentially requiring significant computational resources. Second, the accuracy of the results is highly dependent on the quality and quantity of the training data, which can be a limiting factor in some scenarios. Lastly, while PINNs show promise in generalizing across different physical phenomena, there is still a need for further validation in diverse and untested scenarios to fully establish their robustness and reliability.

4. Model scalability

The PINNs model can be used for more complex biological and surgical intervention simulations such as cardiovascular blood flow simulations, cryosurgeries, hyperthermia cancer treatment, drug delivery, and pharmacokinetics where precise modeling of non-linear and dynamic systems is crucial. PINNs integrate differential equations that describe these processes directly into the neural network framework,

enabling the simulation of complex interactions and responses under varying physiological conditions. This integration helps in optimizing therapeutic strategies and improving surgical outcomes by providing real-time predictive insights and adapting to changes during the procedure, thus ensuring higher precision and efficacy in patient-specific treatments. As the complexity of the mechanical system increases, so does the complexity of the neural network model demanding for faster and more powerful computer hardware. The mentioned challenge may be addressed using distributed computing or using more advanced methods such as adaptive activation function which may reduce the complexity of the system hence the need for more computation power. Another option to tackle the performance challenge would be to use the high-performance computing cloud services which provide substantial GPU capabilities. The cloud services are good solutions for on demand analysis of complex systems as the cost of computation could be significantly less than purchasing the hardware, software, and the energy to run the PINNs model.

5. Conclusions

The developed PINNs model, which demonstrates comparable accuracy to conventional CFD approaches, can offer invaluable insights into the solidification patterns during the freeze-casting scaffold fabrication. Remarkably, such a promising performance was achieved with significantly fewer pre-determined boundary conditions than the numerical methods such as CFD for which a complete knowledge of all the boundary conditions is essential.

In future work, we plan to extend the capabilities of the PINNs model to establish a more comprehensive correlation between experimental parameters—including temperature and mold geometry—and the resulting scaffold characteristics, such as average pore size and morphology. By incorporating these additional parameters into the model, we aim to predict the microstructural outcomes of various freeze-casting conditions more accurately. This expansion will involve setting up controlled experiments to gather relevant data on the effects of temperature gradients and mold shapes on scaffold properties, which can then be used to further refine and validate the PINNs model.

The complexity of transient solidification, characterized by the incompletely defined boundary conditions, limits the utility of conventional numerical approaches while unveiling a fresh avenue of research using advanced machine learning algorithms to study complex experiments such as freeze casting. Herein, we considered 5000 data points in space and time, equivalent to a staggering 250,000 timesteps. This is akin to monitoring the temperature values at only two selected boundary points at every 50 timesteps. In

other words, deploying a temperature probe capable of recording at a 2 Hz frequency at a random boundary location, the model can remarkably predict the temperature distribution and solidification within the whole domain at all time instances, with an impressive level of accuracy. This unique utility holds the promise of reliably designing biomaterial scaffolds suitable for cell growth, mobility, and nutrient delivery, with finely tuned microstructures required in various tissue engineering applications, all while reducing fabrication cost and time.

Data availability statement

The data cannot be made publicly available upon publication because no suitable repository exists for hosting data in this field of study. The data that support the findings of this study are available upon reasonable request from the authors.

ORCID iDs

Amir Rouhollahi  <https://orcid.org/0000-0002-7299-7394>

Amin Ebrahimi  <https://orcid.org/0000-0002-4912-2549>

References

- [1] Hernandez J L and Woodrow K A 2022 Medical applications of porous biomaterials: features of porosity and tissue-specific implications for biocompatibility *Adv. Healthc. Mater.* **11** 2102087
- [2] Jang T *et al* 2022 Topography-supported nanoarchitectonics of hybrid scaffold for systematically modulated bone regeneration and remodeling *Adv. Funct. Mater.* **32** 2206863
- [3] Wu S, Xu J, Zou L, Luo S, Yao R, Zheng B, Liang G, Wu D and Li Y 2021 Long-lasting renewable antibacterial porous polymeric coatings enable titanium biomaterials to prevent and treat peri-implant infection *Nat. Commun.* **12** 3303
- [4] Zhang H, Hussain I, Brust M, Butler M F, Rannard S P and Cooper A I 2005 Aligned two- and three-dimensional structures by directional freezing of polymers and nanoparticles *Nat. Mater.* **4** 787–93
- [5] Deville S, Tomsia A P and Meille S 2022 Complex composites built through freezing *Acc. Chem. Res.* **55** 1492–502
- [6] Lee H, Lee M-K, Han G, Kim H-E, Song J, Na Y, Yoon C-B, Oh S, Jang T-S and Jung H-D 2022 Customizable design of multiple-biomolecule delivery platform for enhanced osteogenic responses via ‘tailored assembly system *Bio-Des. Manuf.* **5** 451–64
- [7] Yin T J and Naleway S E 2023 Freeze casting with bioceramics for bone graft substitutes *Biomed. Mater. Devices* **1** 366–87
- [8] Rouhollahi A, Ilegbusi O, Florczyk S, Xu K and Foroosh H 2020 Effect of mold geometry on pore size in freeze-cast chitosan-alginate scaffolds for tissue engineering *Ann. Biomed. Eng.* **48** 1090–102
- [9] Munch E, Launey M E, Alsem D H, Saiz E, Tomsia A P and Ritchie R O 2008 Tough, bio-inspired hybrid materials *Science* **322** 1516–20
- [10] Deville S 2008 Freeze-casting of porous ceramics: a review of current achievements and issues *Adv. Eng. Mater.* **10** 155–69
- [11] Lloreda-Jurado P J, Chicardi E, Paúl A and Sepúlveda R 2021 Effect of processing parameters on the properties of freeze-cast Ni wick with gradient porosity *Mater. Des.* **206** 109795

- [12] Arai N and Faber K T 2021 Freeze-cast honeycomb structures via gravity-enhanced convection *J. Am. Ceram. Soc.* **104** 4309–15
- [13] Conde-González A, Glinka M, Dutta D, Wallace R, Callanan A, Oreffo R O C and Bradley M 2023 Rapid fabrication and screening of tailored functional 3D biomaterials: Validation in bone tissue repair—Part II *Biomater. Adv.* **145** 213250
- [14] Lee J and Deng Y 2011 The morphology and mechanical properties of layer structured cellulose microfibril foams from ice-templating methods *Soft Matter* **7** 6034–40
- [15] Zhang H and Cooper A I 2007 Aligned porous structures by directional freezing *Adv. Mater.* **19** 1529–33
- [16] Qin K, Parisi C and Fernandes F M 2021 Recent advances in ice templating: from biomimetic composites to cell culture scaffolds and tissue engineering *J. Mater. Chem. B* **9** 889–907
- [17] Scotti K L and Dunand D C 2018 Freeze casting—a review of processing, microstructure and properties via the open data repository, FreezeCasting.net *Prog. Mater. Sci.* **94** 243–305
- [18] Shao G, Hanaor D A H, Shen X and Gurlo A 2020 Freeze casting: from low-dimensional building blocks to aligned porous structures—a review of novel materials, methods, and applications *Adv. Mater.* **32** 1907176
- [19] Zhu X et al 2020 Precise control of versatile microstructure and properties of graphene aerogel via freezing manipulation *Nanoscale* **12** 4882–94
- [20] Li W L, Lu K and Walz J Y 2012 Freeze casting of porous materials: review of critical factors in microstructure evolution *Int. Mater. Rev.* **57** 37–60
- [21] Yang C, Zhu X, Wang X, Wang J and Huang H 2019 Phase-field model of graphene aerogel formation by ice template method *Appl. Phys. Lett.* **115** 111901
- [22] Huang T-H, Huang T-H, Lin Y-S, Chang C-H, Chen P-Y, Chang S-W and Chen C-S 2018 Phase-field modeling of microstructural evolution by freeze-casting *Adv. Eng. Mater.* **20** 1700343
- [23] Ramšak M, Ravnik J, Zadavec M, Hrberšek M and Iljaž J 2017 Freeze-drying modeling of vial using BEM *Eng. Anal. Bound. Elem.* **77** 145–56
- [24] Szilágyi B and Nagy Z K 2016 Graphical processing unit (GPU) acceleration for numerical solution of population balance models using high resolution finite volume algorithm *Comput. Chem. Eng.* **91** 167–81
- [25] Barr S A and Luijten E 2010 Structural properties of materials created through freeze casting *Acta Mater.* **58** 709–15
- [26] Yamamoto T 2009 Computer modeling of polymer crystallization—Toward computer-assisted materials' design *Polymer* **50** 1975–85
- [27] Peppin S S L, Elliott J a W and Worster M G 2006 Solidification of colloidal suspensions *J. Fluid Mech.* **554** 147–66
- [28] Lian G, Moore S and Heeney L 2006 Population balance and computational fluid dynamics modelling of ice crystallisation in a scraped surface freezer *Chem. Eng. Sci.* **61** 7819–26
- [29] Muzzio C R and Dini N G 2011 Simulation of freezing step in vial lyophilization using finite element method *Comput. Chem. Eng.* **35** 2274–83
- [30] Husmann A, Pawelec K, Burdett C, Best S and Cameron R 2015 Numerical simulations to determine the influence of mould design on ice-templated scaffold structures *J. Biomed. Eng. Inform.* **1** 47
- [31] Rouhollahi A, Ilegbusi O, Florczyk S, Xu K and Foroosh H 2019 Effect of mold geometry on pore size in freeze-cast chitosan-alginate scaffolds for tissue engineering *Ann. Biomed. Eng.* **48** 1090–102
- [32] Cyr J A, Husmann A, Best S M and Cameron R E 2022 Complex architectural control of ice-templated collagen scaffolds using a predictive model *Acta Biomater.* **153** 260–72
- [33] Li S, Wang G, Di Y, Wang L, Wang H and Zhou Q 2023 A physics-informed neural network framework to predict 3D temperature field without labeled data in process of laser metal deposition *Eng. Appl. Artif. Intell.* **120** 105908
- [34] Zhao X, Gong Z, Zhang Y, Yao W and Chen X 2023 Physics-informed convolutional neural networks for temperature field prediction of heat source layout without labeled data *Eng. Appl. Artif. Intell.* **117** 105516
- [35] Zobeiry N and Humfeld K D 2021 A physics-informed machine learning approach for solving heat transfer equation in advanced manufacturing and engineering applications *Eng. Appl. Artif. Intell.* **101** 104232
- [36] Amini Niaki S, Haghghat E, Campbell T, Poursartip A and Vaziri R 2021 Physics-informed neural network for modelling the thermochemical curing process of composite-tool systems during manufacture *Comput. Methods Appl. Mech. Eng.* **384** 113959
- [37] Hughes M T, Kini G and Garimella S 2021 Status, challenges, and potential for machine learning in understanding and applying heat transfer phenomena *J. Heat Transf.* **143** 120802
- [38] Seifert A, Gruber J, Gbureck U and Groll J 2022 Morphological control of freeze-structured scaffolds by selective temperature and material control in the ice-templating process *Adv. Eng. Mater.* **24** 2100860
- [39] Li Z, Liu L, Zhang Y and Zhou G 2016 Influence of crucible thermal conductivity on crystal growth in an industrial directional solidification process for silicon ingots *Int. J. Photoenergy* **2016** e8032709
- [40] Yang G, Kubota N, Sha Z, Louhi-Kultanen M and Wang J 2006 Crystal shape control by manipulating supersaturation in batch cooling crystallization *Cryst. Growth Des.* **6** 2799–803
- [41] Petzold G and Aguilera J M 2009 Ice morphology: fundamentals and technological applications in foods *Food Biophys.* **4** 378–96